5-1-2004

Dynamic Correction of a Distorted Image Using a Photorefractive Polymeric Composite

Jeffrey G. Winiarz
Missouri University of Science and Technology, winiarzj@mst.edu

Fassil Ghebremichael

Jayan Sanders Thomas

Gerald R. Meredith

et. al. For a complete list of authors, see http://scholarsmine.mst.edu/chem_facwork/454

Recommended Citation

J. G. Winiarz et al., "Dynamic Correction of a Distorted Image Using a Photorefractive Polymeric Composite," *Optics Express*, vol. 12, no. 11, pp. 2517-2528, Optical Society of American, May 2004.
The definitive version is available at https://doi.org/10.1364/OPEX.12.002517

Dynamic correction of a distorted image using a photorefractive polymeric composite

Jeffrey G. Winiarz and F. Ghebremichael

Laser and Optics Research Center, Department of Physics, U.S. Air Force Academy, Colorado 80840
Fassil.Ghebremichael@usafa.af.mil

Jayan Thomas, Gerald Meredith, and Nasser Peyghambarian

Optical Sciences Center, University of Arizona, Tucson, Arizona 85721

Abstract: We demonstrate, for the first time, the dynamic correction of aberrated images in real-time using a polymeric composite with fast response times. The current novel experimental design is capable of restoring a phase aberrated, image carrying laser beam, to nearly its original quality. The ability to reconstruct images in real-time is demonstrated through the changing of the aberrating medium at various speeds. In addition, this technique allows for the correction of images in motion, demonstrated through the oscillatory movement of the resolution target. We also have demonstrated that important parameters of the materials in the study such as response times, diffraction efficiencies and optical gains all retain high figures of merit values under the current experimental conditions.

OCIS codes: (050.7330) Volume holographic gratings; (090.1000) Aberration compensation; (100.3020) Image reconstruction-restoration; (190.5330) Photorefractive nonlinear optics

References and links

1. Y. Yitzhaky, I. Dror, and N. S. Kopeika, "Restoration of atmospherically blurred images according to weather-predicted atmospheric modulation transfer function," Opt. Eng. **36**, 3064-3072 (1997).
2. M. C. Gower, "Phase conjugation," J. Mod. Optic. **35**, 449-472 (1988).
3. C. L. Hayes, R. A. Brandewie, W. C. Davis, and G. E. Mevers, "Experimental test of an infrared phase conjugation adaptive array," J. Opt. Soc. Am. **67**, 269-277 (1977).
4. W.-J. Joo, N.-J. Kim, H. Chun, I. K. Moon, and N. Kim, "Polymeric photorefractive composite for holographic applications," Polymer **42**, 9863-9866 (2001).
5. T. Baade, A. Kiessling, and R. Kowarschik, "A simple method for image restoration and image pre-processing using two-wave mixing in $Bi_{12}TiO_{20}$," J. Opt. A-Pure Appl. Op. **3**, 250-254 (2001).
6. A. N. Simonov, A. V. Larichev, V. P. Shibaev, and A. I. Stakhanov, "High-quality correction of wavefront distortions using low-power phase conjugation in azo dye containing LC polymer," Opt. Commun. **197**, 175-185 (2001).
7. A. Brignon, J.-P. Huignard, M. H. Garrett, and I. Mnushkina, "Spatial beam cleanup of a Nd:YAG laser operating at 1.06 μm with two-wave mixing in $Rh:BaTiO_3$," Appl. Opt. **36**, 7788-7793 (1997).
8. A. E. Chiou and P. Yeh, "Laser-beam cleanup using photorefractive two-wave mixing and optical phase conjugation," Opt. Lett. **11**, 461-463 (1986).
9. A. E. T. Chiou and P. Yeh, "Beam cleanup using photorefractive two-wave mixing," Opt. Lett. **10**, 621-623 (1985).
10. B. Kippelen, K. Meerholz, Sandalphon, B. L. Volodin, and N. Peyghambarian, "Photorefractive polymers and their applications," Mol. Cryst. Liq. Cryst. Sci. Technol., Sect. A **283**, 109-114 (1996).
11. W. E. Moerner and S. M. Silence, "Polymeric photorefractive materials," Chem. Rev. **94**, 127-155 (1994).
12. V. L. Vinetskii, N. V. Kukhtarev, S. G. Odulov, and M. S. Soskin, "Dynamic self-diffraction of coherent light beams," Uspekhi Fizicheskikh Nauk **129**, 113-137 (1979).
13. D. L. Staebler and J. J. Amodei, "Coupled-wave analysis of holographic storage in lithium niobate," J. Appl. Phys. **34**, 1042-1049 (1972).
14. G. S. Agarwal and E. Wolf, "Theory of phase conjugation with weak scatterers," J. Opt. Soc. Am. **72**, 321 (1982).

#4015 - $15.00 US Received 11 March 2004; revised 24 May 2004; accepted 25 May 2004

15. J. Zhang, S. Yoshikado, and T. Aruga, "Distorted image reconstruction using photorefractive effects," Journal of the Communications Research Laboratory **49**, 67-71 (2002).
16. M. Tziraki1, R. Jones, P. M. W. French, M. R. Melloch, and D.D. Nolte, "Photorefractive holography for imaging through turbidmedia using low coherence light," Appl. Phys. B **70**, 151–154 (2000).
17. S. C. W. Hyde, N. P. Barry, R. Jones, J. C. Dainty, P. M. W. French, M. B. Klein, and B. A. Wechsler, "Depth-resolved holographic imaging through scattering media by photorefraction," Opt. Lett. **20**, 1331-1334 (1995).
18. E. Leith, H. Chen, Y. Chen, D. Dilworth, J. Lopez, R. Masri, J. Rudd, and J. Valdmanis, "Electronic holography and speckle methods for imaging through tissue using femtosecond gated pulses," Appl. Opt. **30**, 4204-4210 (1991).
19. K. G. Spears, J. Serafin, N. H. Abramson, X. Zhu, and H. Bjelkhagen, "Chrono-coherent imaging for medicine," in *Proceedings of IEEE Conference on Trans. Biomed. Eng.* (Institute of Electrical and Electronics Engineers, New York, 1989), pp. 1210-1221.
20. N. H. Abramson and K. G. Spears "Single pulse light-in-flight recording by holography" Appl. Opt . **28**, 1834-1841 (1989).
21. M. A. Duguay and A. T. Mattick, "Untrahigh speed photography of picosecond light pulses and echoes," Appl. Opt. **10**, 2162-2171 (1971).
22. E. Hendrickx, Y. Zhang, K. B. Ferrio, J. A. Herlocker, J. Anderson, N. R. Armstrong, E. A. Mash, A. P. Persoons, N. Peyghambarian, and B. Kippelen, "Photoconductive properties of PVK-based photorefractive polymer composites doped with fluorinated styrene chromophores," J.Mater.Chem **9**, 2251-2258 (1999).
23. J. W. Goodman, *Introduction to Fourier Optics* (McGraw-Hill, San Francisco, 1968).
24. D. Wright, M. A. Díaz-García, J. D. Casperson, M. DeClue, W. E. Moerner, and R. J. Twieg, "High-speed photorefractive polymer composites," Appl. Phys. Lett. **73**, 1490-1492 (1998).
25. S. H. Chung and J. R. Stevens, "Time-dependent correlation and the evaluation of the stretched exponential or Kohlrausch–Williams–Watts function," Am. J. Phys. **11**, 1024-1030 (1991).
26. J. G. Winiarz, L. Zhang, M. Lal, C. S. Friend, and P. N. Prasad, "Observation of the photorefractive effect in a hybrid organic-inorganic nanocomposite," J. Am. Chem. Soc. **121**, 5287-5295 (1999).
27. B. Swedek, N. Cheng, Y. Cui, J. Zieba, J. Winiarz, and P. N. Prasad, "Temperature-dependence studies of photorefractive effect in a low glass-transition-temperature polymer composite," J. Appl. Phys. **82**, 5923-5931 (1997).
28. Y. Cui, B. Swedek, N. Cheng, J. Zieba, and P. N. Prasad, "Dynamics of photorefractive grating erasure in polymeric composites," J. Appl. Phys. **85**, 38-43 (1999).
29. H. Kogelnik, "Coupled Wave Theory for Thick Hologram Gratings," Bell Syst. Tech. J. **48**, 2909-2945 (1969).

1. Introduction

A spatially clean laser beam is exceedingly crucial for many applications of interest such as interference, target identification and high resolution applications. This is especially true for information-carrying beams. Even with the utmost care, however, the quality of a beam may become unacceptably distorted due to intrinsically imperfect optics or irregularities in the propagation medium. In applications requiring the transmission of a laser beam over long distances through a distorting medium such as the atmosphere, the primary mechanism of degradation can be attributed to turbulence resulting in wave-front skew which can be on the order of tens to hundreds of microradians [1]. Consequentially, the information carrying beam is spatially distorted and shifting of the image in the image plane occurs. This can involve either the shifting of the entire image or, alternatively, parts of the image with respect to one another. A variety of means have been formulated to compensate for beam/image distortions. As early as the 1970s the construction of adaptive optical elements, capable of manipulating light subsequent to propagation through turbulent media, was the motivation for investigations involving phase compensating mirrors (windows) operating under electro-optical or mechanical principles [2,3]. Such adaptive optical elements have been utilized in a variety of applications including targeting over long distances with high-power laser beams as well as in astronomical telescopes. The resolving power of such adaptive optics, however, is limited by the finite size of the actuators. In addition, the essential wave-front detection systems in electro-optical and mechanical adaptive optical elements make them inherently slow, expensive and complicated.

#4015 - $15.00 US Received 11 March 2004; revised 24 May 2004; accepted 25 May 2004

In an effort to surmount these shortcomings, all-optical methods of beam-cleanup, especially those involving two-beam-coupling (TBC) and four-wave-mixing (FWM) in photorefractive (PR) materials, have become of great interest [4-9]. The phenomenon of photorefractivity in polymeric composites can be realized in materials which simultaneously exhibit photoconductive and electro-optic properties [9-13]. It should be noted that while these properties are necessary for the observation of the photorefractive effect, their presence does not necessarily imply that a particular material will possess photorefractive properties. Photoconductivity allows for the formation of an internal space-charge electric field through a subsequent combination of photogeneration, transport, and trapping of charge carriers. When two coherent laser beams with similar polarization components, intersect in a PR medium, a spatially periodic intensity pattern will ensue. In the bright regions, the generation of photocharges will occur followed by the subsequent migration of these charges (sometimes enhanced with an externally applied electric field) into the darker regions of the illumination pattern. In the case of polymeric composites, holes are almost always the dominant mobile charge-carrier. This process results in the establishment of a space-charge field, E_{SC}.

In materials exhibiting electro-optic (EO) activity, the ensuing space-charge field will induce a spatial modulation in the index of refraction. In polymeric materials EO activity is ordinarily accomplished through the addition of a second-order nonlinear dye, capable of exhibiting the electronic Pockels effect. However, a strong birefringence contribution (due to the dipolar reorientation of the chromophores) often provides the dominant contribution to, and may in fact, be solely responsible for, the overall modulation of the refractive index. The resulting manifestation of these processes is light induced phase grating (hologram). Photorefractive holograms are generated in the form of a refractive index grating written by the interference pattern generated when two laser beams are crossed in the medium which can then be retrieved through the diffraction of a probe beam. An unusual feature of a photorefractive grating is the phase shift between the intensity pattern (intensity of the overlapped beams) and the resulting periodic refractive index modulation. This phenomenon gives rise to asymmetric energy transfer in two-beam coupling experiments wherein one beam gains intensity at the expense of the other.

When the PR properties of composite samples are studied via FWM techniques using an oblique experimental setup, holographic gratings are written through the intersection of two coherent beams generated by a laser typically operating with *s*-polarization. Normally, a much weaker *p*-polarized reading beam propagates in a direction opposite of one of the writing beams. The grating formed through the intersection of the writing beams subsequently diffracts a portion of the reading, or probe beam, which can then be monitored by a photodetector. From the data obtained in this experiment, several characteristics concerning the composite material and the grating formed within the material can be ascertained.

While the coupling of the beams' energy has been described in the literature in detail, far fewer studies have focused on the relative phases of the coupled beams. The absence of phase cross-talk has been demonstrated in PR inorganic crystals and has been described in terms of diffraction from a holographic refractive index grating in a PR medium [9].

The idea of a PR medium for the cleanup of a phase distorted laser beam as well as the reconstruction of an aberrated image has been demonstrated in a variety of systems. The cleaning of a phase distorted laser beam was originally verified using a two-wave mixing geometry [8,9]. Alternatively, the effects of a phase aberrating medium on an image carrying beam can be eliminated using a PR device such as a phase conjugate mirror [14]. In this case the distorted beam is redirected back through the phase distorting medium in the reverse direction. This propagation phase conjugate cancels the forward propagation phase through the distorter and the beam is restored very nearly to its original quality. This scheme, however, suffers from the serious drawback in that the image carrying beam must be passed through the distorter twice, and places the corrected image on the same side of the distorting medium from which it had originated. Thus this image correcting scheme has enjoyed little practical application since it is not useful in the transmission of an image from one side of a

#4015 - $15.00 US Received 11 March 2004; revised 24 May 2004; accepted 25 May 2004

distorting medium to the other. Other schemes employing phase conjugate mirrors requiring only a single pass through the aberrating medium have been devised which use glint or guidestar techniques. These techniques, however, suffer from the current inability to construct practical phase conjugate mirrors. More recently, single-pass transmission schemes have been devised for imaging through turbid media using PR materials and pulsed laser sources [15-21]. These techniques are often referred to as "coherence gating techniques." In these instances low coherence light is split into an object beam and a reference beam followed by the subsequent passing of the object beam through a turbid medium. By adjusting the delay of the reference beam such that its arrival at the PR medium coincides temporally with the arrival of the early arriving ballistic (unscattered) photons of the object beam, only the least corrupted, image bearing photons, contribute to the hologram [16]. However, in many scenarios involving wave-front skew there are no ballistic photons which can be distinguished from those which carry distorted information.

In this communication we demonstrate the use of a PR composite to restore an image subjected to temporally varying aberrations. Moreover, a tailored forward FWM geometry permitted the correction of a continuously varying image. The setup consisted of an *s*-polarized beam that was split into an object and reference beam. The object beam was subsequently passed through a half wave-plate which slightly rotated the beam's polarization relative to the pure *s*-polarization, effectively dividing it into two beams; a larger *s*-polarized component that served as a writing beam and a smaller *p*-polarized component that served as a probe beam. The object beam was then passed through a spatial light modulator that was translated in a direction perpendicular to the beam path and finally through a phase aberrator. The phase aberrator was likewise translated in a direction perpendicular to the object beam. The aberrated object beam then interfered with the reference beam in the photorefractive sample, writing a grating. Consequently, a portion of the object beam was diffracted into the path of the reference beam. A polarizing beam splitter was then used to pick out the *p*-polarized component, originating solely from the object beam. This beam was ultimately sent to a CCD camera where the corrected beam was imaged. The quality of the corrected image depended upon the speed of the translated aberrator with a noticeable improvement occurring as the translation speed of the aberrator was slowed. We also have used this and TBC configurations to study the diffraction efficiencies, response times and TBC coefficients.

2. Experimental

For all experiments described herein the wavelength, λ, was the 633 nm line of a HeNe laser. The intersecting beams (I_{ref} and I_{obj}) formed an angle of ~36˚ in air and the sample normal formed an angle of ~48˚ with the beam bisector. It was empirically established that these angles optimized the outcome (i.e. resolution, efficiency and response time) of the experiments in question. A novel forward FWM geometry was used for all imaging experiments as well as those involving the measurement of the diffraction efficiencies, η.

A detailed representation of the experimental configuration is given in Fig. 1. An *s*-polarized HeNe laser beam was split into an object and reference beam (I_{obj} and I_{ref}, respectively). A lens, L_1, was used to adjust the beam size of I_{ref} such that it matched that of I_{obj} at the sample. In order to maintain the approximate plane-wave nature of I_{ref} at the sample, L_1 had a relatively long focal length (f_{L1} = 1 m). The beam sizes I_{obj} and I_{ref} at the sample were ~0.05 cm with both beams adjusted to a power of ~3.1 mW. Thus at the sample $I_{ref} \approx I_{obj} \approx 63$ mW/cm^2. I_{obj} initially was passed through $(\lambda/2)_2$ which slightly rotated the beam. For all experiments the degree of polarization rotation, θ, of I_{obj} was -12° (when looking in the same direction as the beam is traveling) from the pure *s*-polarization, unless otherwise stated. Through this means, I_{obj} was effectively made to be comprised of two beams; a larger *s*-polarized component, $I_{obj,s}$, which serves as a writing beam and a smaller *p*-polarized component, $I_{obj,p}$, which serves as a probe beam.

Subsequently I_{obj} passed through a spatial light modulator, in this case an Air Force resolution target, AF, which was moved back and forth in a direction perpendicular to the

#4015 - $15.00 US Received 11 March 2004; revised 24 May 2004; accepted 25 May 2004

beam path. The distance traversed by AF in one back and forth cycle was ~0.15 cm at a rate of ~22 cycles/min. I_{obj} then encountered a phase aberrator, AB, which was fabricated from a rough plastic sheath. The aberrator was also translated in a direction perpendicular to the beam's path with speeds ranging from ~2 μm/s to ~500 μm/s. The aberrated I_{obj} then interfered with I_{ref} in the PR sample, writing a grating. Consequently a portion of I_{obj} was diffracted into the path of I_{ref}. A portion of I_{ref} was also transmitted through the sample in the same path as the diffracted portion of I_{obj}. At the polarizing beam splitter, PBS, $I_{obj,s}$ and I_{ref} were "filtered out" and $I_{obj,p}$, originating solely from the object beam, was sent to the CCD camera (or PD1) where the corrected beam was imaged. It is noted the experimental scheme as depicted in Fig. 1 would have to be modified for practical applications. This is due to the fact that in realistic applications I_{ref} would posses the same aberrations as those found in by I_{obj}. This modification can be easily accomplished through the insertion of a spatial modulator (pinhole) in the path of I_{ref}, such that a clean, plane-wave portion of the reference beam is obtained. Through this technique I_{ref} will retain its coherence with respect to I_{obj}. Lenses L_2–L_5 were incorporated so that the image plane of the Air Force resolution target coincided with the CCD camera as well as to permit a degree of control over the beam diameter. While L_2–L_5 were required only for the imaging experiments, they were left in place for all experiments and characterizations referenced in this communication.

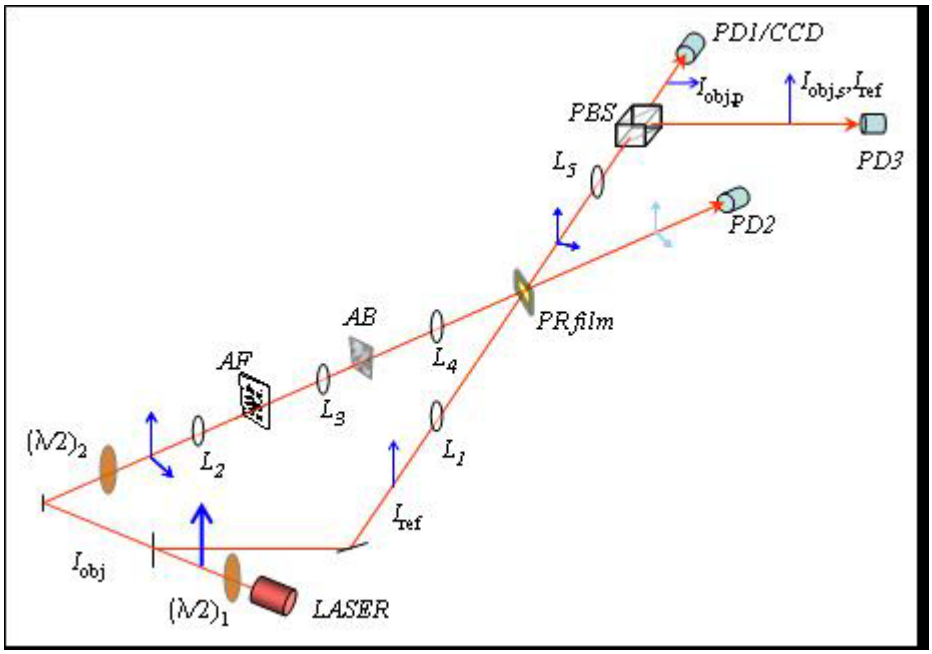

Fig. 1. (1.68 MB) Schematic diagram depicting the experimental setup used for PR characterizations. The number in parentheses is the position of each relevant optical element with respect to the sample where negative (positive) numbers denote the input (output) side of the sample along the appropriate beam path. $(\lambda/2)_1$, $(\lambda/2)_2$, half-wave plates (-200 cm, -70 cm, respectively); $L_{1\text{-}5}$, Lens, f_{L1} = 100 cm, f_{L2} = 15 cm, f_{L3} = 10 cm, f_{L4} = 7.5 cm, f_{L5} = 20 cm (-70 cm, -54.7 cm, -31.2 cm, -13.7 cm, 16.1 cm, respectively); AF, Air Force resolution target (-34.3 cm); AB, phase aberrating medium (-30.4 cm); PBS, polarizing beam splitter; PD, photodiode; CCD, charge-coupled-device camera (145 cm).

For the FWM efficiency studies, the same forward FWM geometry described for the imaging experiments was used. For TBC characterizations the same experimental configuration was employed as that used in the imaging experiments with the following exceptions: The half-wave plate $(\lambda/2)_1$ was configured such that the output radiation was

#4015 - $15.00 US Received 11 March 2004; revised 24 May 2004; accepted 25 May 2004

either *p*-polarized or *s*-polarized and $(\lambda/2)_2$ was appropriately adjusted such that the output polarization remains identical to the input polarization. In addition, the polarizing beam-splitter was removed in order to monitor the intensity of transmitted beams at PD1 and PD2.

The PR medium used in this study was a polymeric composite consisting of the photoconducting polymer matrix poly(*N*-vinylcarbazole) (PVK) which has been doped with the nonlinear optical chromophore 4-homopiperidinobenzylidenemalononitrile (7-DCST) [22], the plasticizer 9-Ethylcarbazole (ECZ), and the photosensitizer C_{60}. In this sample the components PVK:7-DCST:ECZ:C_{60} were in the ratio 49.5:35:15: 0.5 wt% possessing a glass transition temperature of 13˚C, which classifies this composite as a low-T_g material. The sample was 110 μm thick and in an ITO/polymer composite/ITO sandwich geometry, where ITO is indium tin oxide, a transparent conductor. A comprehensive description of the sample fabrication and the performance characteristics of the material can be found elsewhere [22].

3. Results and Discussion

The primary motivation for these experiments deals with the use of a PR composite in the restoration of continuously shifting images subject to temporally varying aberrations. A formal mathematical explanation of the processes at work can be derived parallel to the description in literature as follows [23]: In a corrective hologram, the relevant intensity forming the grating can be described by the equation

$$\left|U_{\text{obj}}\Psi_{\text{ab}} + U_{\text{ref}}\right|^2 = I_{\text{obj}} + I_{\text{ref}} + U_{\text{obj}}\Psi_{\text{ab}}U_{\text{ref}}^* + U_{\text{obj}}^*\Psi_{\text{ab}}^*U_{\text{ref}}, \qquad (1)$$

where U_{ref} and U_{obj} are the amplitudes of the reference and object beams, respectively. Ψ_{ab} ($|\Psi_{\text{ab}}|^2 = 1$) is the phase information added to U_{obj} after passing through the aberrator, neglecting amplitude attenuations. In this formalism we have used $|U|^2 = I$. In standard holography the phase information (virtual image) can be recovered by sending a reference beam, U_{ref}, to reconstruct the identical phase information. In our case, we first use U_{obj} to show the aberration effect, revealed in the last term of the equation

$$U_{\text{obj}}\left|U_{\text{obj}}\Psi_{\text{ab}} + U_{\text{ref}}\right|^2 = I_{\text{obj}}U_{\text{obj}} + I_{\text{ref}}U_{\text{obj}} + U_{\text{obj}}^2U_{\text{ref}}^*\Psi_{\text{ab}} + I_{\text{obj}}U_{\text{ref}}\Psi_{\text{ab}}^*, \qquad (2)$$

(note: it is the phase conjugate of the aberrator information). We then use $U_{\text{obj}}\Psi_{\text{ab}}$ to effectively remove aberration, evidenced in the last term of the equation

$$\begin{aligned} U_{\text{obj}}\Psi_{\text{ab}}\left|U_{\text{obj}}\Psi_{\text{ab}} + U_{\text{ref}}\right|^2 = {} & I_{\text{obj}}U_{\text{obj}}\Psi_{\text{ab}} \\ & + I_{\text{ref}}U_{\text{obj}}\Psi_{\text{ab}} + U_{\text{obj}}^2\Psi_{\text{ab}}^2U_{\text{ref}}^* + U_{\text{ref}}I_{\text{obj}} \end{aligned} \qquad (3)$$

where the phase information associated with the distorter is removed.

The ability to accomplish this task is demonstrated in Fig. 2 which depicts images (a-h) taken with aberrator speeds, σ, ranging from σ = 0.0025 mm/s to σ = 0.32 mm/s. The corrected images were obtained using the experimental arrangement described in Fig. 1. The magnitude of the externally applied electric field, *E*, for all imaging experiments was 81.8 V/μm. The uncorrected images were obtained using the same configuration except that the PR sample was replaced by a mirror, allowing for the aberrated reflection to be imaged. Evident in the figure is the fact that the current experimental design is extremely capable of restoring a phase aberrated image to nearly its original quality. The ability to reconstruct images in real time has been demonstrated through the translation of the aberrating medium at a variety of speeds. In addition, this technique allows for the correction of constantly changing images, as demonstrated through the oscillating nature of the resolution target, AF.

Figure 2 also shows that the quality of the corrected image depends upon the speed of the translated aberrator with a noticeable improvement occurring as σ is decreased. While Fig. 2

#4015 - $15.00 US Received 11 March 2004; revised 24 May 2004; accepted 25 May 2004

provides a qualitatively indication of the degradation of the PR signal, Fig. 3 illustrates this point in a quantitative sense. Here the normalized diffraction efficiency is plotted for a variety of aberrator translation speeds. The external steady state diffraction efficiencies, η_0, were calculated according to the equation

$$\eta_0 = I'_{\mathrm{obj,p}} / I_{\mathrm{obj,p}} \ , \tag{4}$$

where $I'_{\mathrm{obj,p}}$ is the diffracted intensity of the *p*-polarization component of I_{obj} as measured by PD1 in Fig. 1 and $I_{\mathrm{obj,p}}$ is the intensity of the *p*-polarization component of I_{obj} as measured prior to the PR sample.

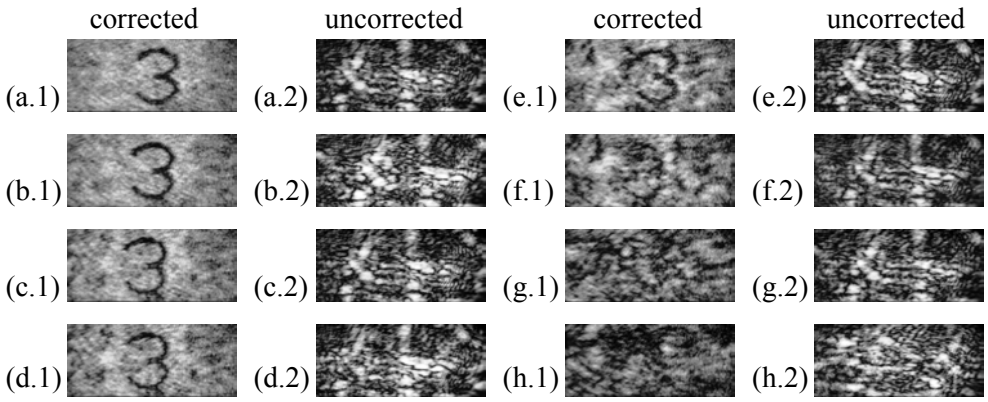

Fig. 2. Corrected and uncorrected images obtained as the aberrator is moved at constant speed. The speed of aberrator translation in the remainder of the frames are as follows (all videos are 1.73 MB in size): a) 0.0025 mm/s; b) 0.0055 mm/s; c) 0.012 mm/s; d) 0.019 mm/s; e) 0.033 mm/s; f) 0.068 mm/s; g) 0.14 mm/s; and h) 0.32 mm/s. E = 85.7 V/μm for all corrected images.

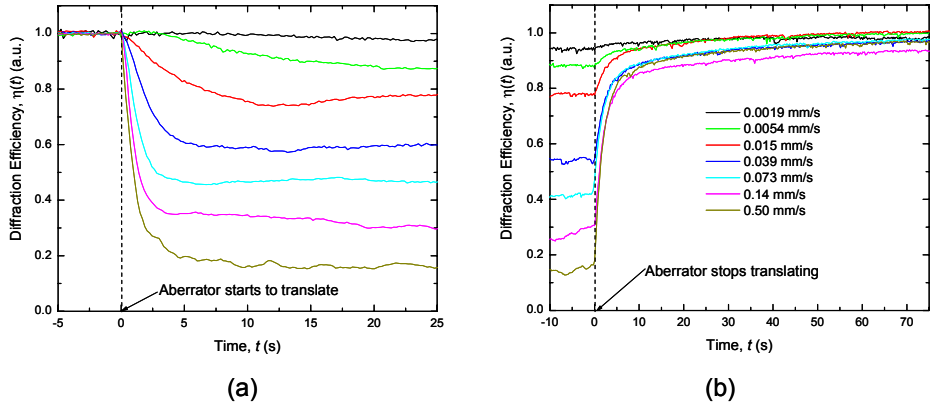

Fig. 3. Change in diffraction signal for various speeds of aberrator translation (E = 85.7 V/μm). (a) temporal decay in the diffraction efficiency as the aberrator begins to translate, (b) temporal growth in the diffraction efficiency as the translation of the aberrator is discontinued.

Evident in the figure is the fact that as σ is increased, the steady state diffraction efficiency, η_0, drops dramatically. When the aberrator is translated at the slowest speed investigated in this communication (σ = 1.9 μm/s), the magnitude of the steady state diffraction efficiency drops to only η_0 ~0.94 of its original value. In contrast, translating the aberrator at a rate of σ = 0.50 mm/s, the fastest rate of translation attempted in this series of experiments, the

#4015 - $15.00 US
Received 11 March 2004; revised 24 May 2004; accepted 25 May 2004

magnitude of diffraction efficiency falls to η_0 ~0.14 of its original value. This observation can be explained as a lagging in the redistribution of charge-carriers within the PR sample with respect to the redistribution of the light as well as a lag associated with the thermal reorientation of the chromophores. The relationship between the diffraction efficiency and velocity of aberrator translation, σ, is depicted in Fig. 4.

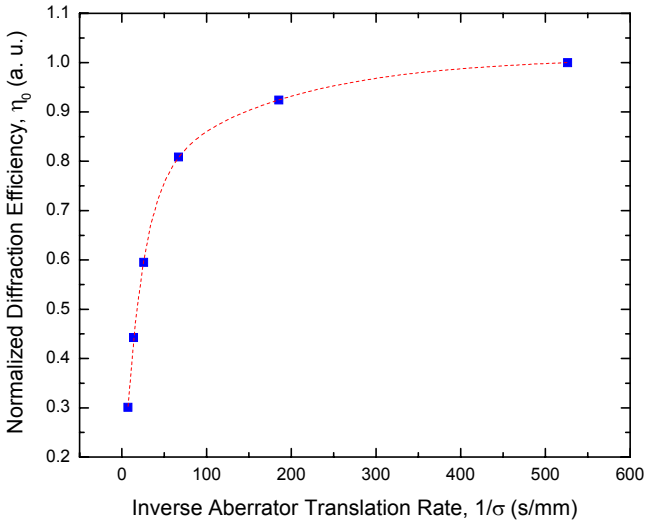

Fig. 4. The the normalized diffraction efficiency, η_0, as a function of the inverse of the rate of translation of the aberrating medium, $1/\sigma$. The line is a guide for the eye.

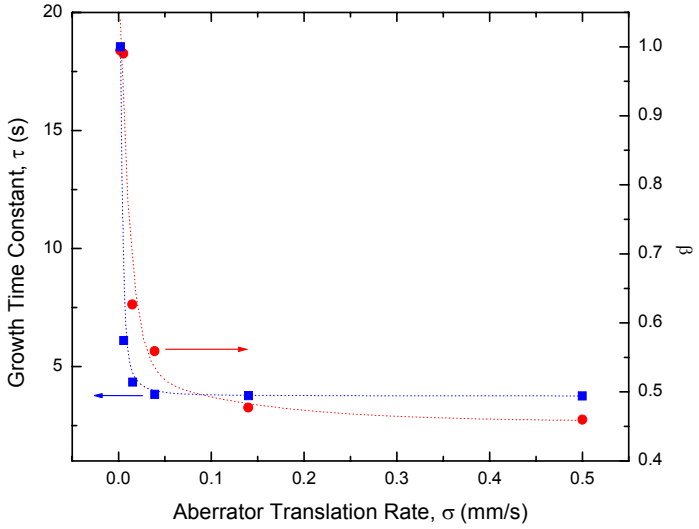

Fig. 5. Growth time constant, τ, and the parameter β as a function of rate of aberrator translation, σ. The lines are guides for eye.

The growth data presented in Fig. 3(a) also permits the quantitative determination of the growth time constants, τ, associated with this PR material under the given experimental conditions. Figure 5 represents information obtained from a stretched exponential fit to the data of Fig. 3(b). The fit equation is given by

#4015 - $15.00 US
Received 11 March 2004; revised 24 May 2004; accepted 25 May 2004

$$\eta(t) = \eta_0 \left\{ 1 - \exp\left[-(t/\tau)^{\beta} \right] \right\} , \quad (5)$$

where β is an indication of the degree to which the rate of increase slows with time [24]. Such stretched exponential behavior is known to ensue when a physical process involves a distribution of time constants with β decreasing as the time constant distribution increases [24,25]. The determined values of β for each σ are also presented in Fig. 5. The stretched exponential behavior associated with the temporal traces of the rise in diffraction efficiencies is not surprising due to the dispersive nature of both the charge transport in such systems as well as realignment of the dipolar chromophores. From Fig. 5 it is apparent that for faster σ, where the diffraction efficiency falls to its minimum values, the values of β also achieve their lowest values, indicating the maximum width of the distribution associated with τ. Conversely, for the lower values of σ, β approaches unity, indicating a very narrow distribution in τ. The data in Fig. 5 also reveals that τ is at a maximum for the slowest σ.

This analysis indicates that when the aberrator is translated quickly (large values of σ) and the diffraction efficiency is allowed to drop significantly, a larger variety of processes are involved in the recovery of η(*t*) compared with when the aberrator is translated slowly and the diffraction efficiency in only minimally effected. Furthermore, since τ decreases for these larger recoveries of η(*t*), one can conclude that the processes more prevalent for the larger recoveries of η(*t*) are the relatively faster processes, likely those associated with the redistribution of charge carriers [11,26-28]. On the other hand, slower σs, associated with minimal changes in η(*t*), results in large values of β, indicating that fewer process are involved in the ultimate recovery of η(*t*). In contrast to the previous scenario, the larger values of τ characteristic of smaller η(*t*) recoveries indicates that the processes implicated are of a slow nature and most likely predominantly attributed to the thermal reorientation of the birefringent/electro-optic chromophores [11,26-28].

Figure 6 presents several videos depicting the rapid movement of the aberrator followed by a sudden stop in its translation. One can see the speed with which the beam is restored to its unaberrated state and the image carried by the beam becomes apparent.

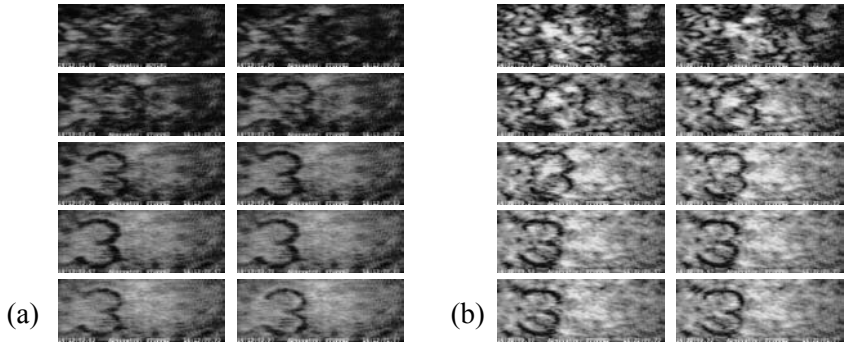

Fig. 6. Videos depicting the rapid movement of the aberrator followed by a sudden stop in its translation. The time stamps present in each frame offer a quantitative indication of the elapsed time. a) (1.19 MB) E = 47.6 V/μm, and b) (1.62 MB) E = 85.7 V/μm.

The performance of the material was also characterized under the current experimental conditions using FWM and TBC techniques. The external steady state diffraction efficiency, η_0, determined via the novel forward FWM geometry described in Fig. 1, for θ = -12°, is presented in Fig. 7 as a function of the externally applied electric field, E. The external steady state diffraction efficiencies, η_0, were calculated according to Eq. (4). Apparent in Fig. 7, for

#4015 - $15.00 US Received 11 March 2004; revised 24 May 2004; accepted 25 May 2004

the greatest applied electric field of E = 85.7 V/μm, a maximum $\eta_0(E)$ of 67.3 % was measured.

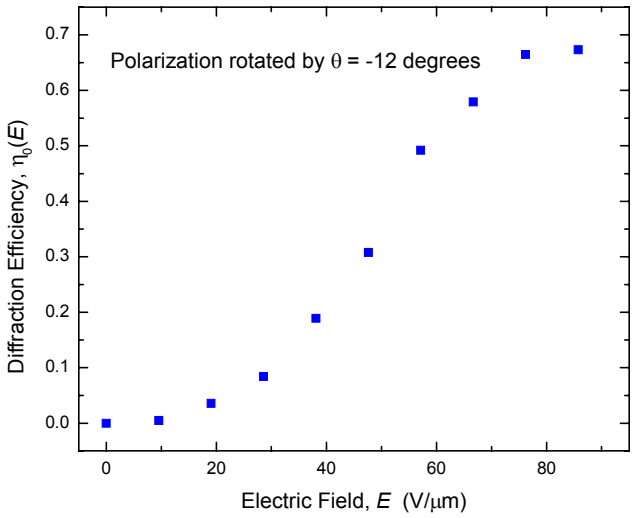

Fig. 7. The external steady state diffraction efficiency, η_0, determined via the novel forward FWM geometry as a function of the externally applied electric field, E. θ = -12°.

In addition to determining η_0 as a function of E, the steady state diffraction efficiencies were also determined at constant E = 85.7 V/μm as a function of θ. For this characterization I_{ref} was maintained at a constant intensity. As was expected, the intensity of the *p*-polarization component of I_{obj} as measured prior to the PR sample, $I_{obj,p}$, assumed a 180° out-of-phase sinusoidal pattern with respect to θ as depicted in Fig. 8(a).

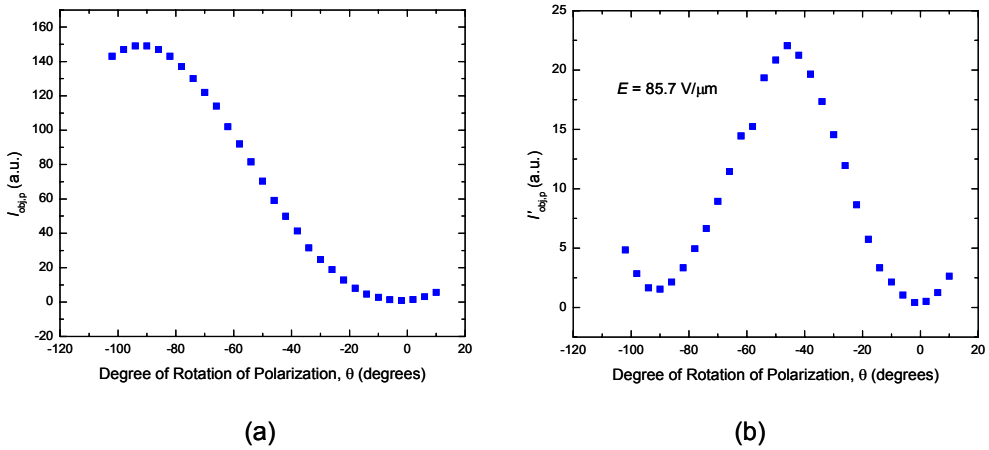

Fig. 8. a) The intensity of the *p*-polarization component of I_{obj} ($I_{obj,p}$) as a function of θ measured prior to the PR sample, and b) the diffracted intensity of I_{obj} ($I'_{obj,p}$) as a function of θ. E = 85.7 V/μm.

The diffracted intensity, $I'_{obj,p}$, measured at PD1 as a function of θ, assumed the characteristics depicted in Fig. 8(b). As with $\eta_0(E)$, $\eta_0(\theta)$ was calculated according to Eq. (4) and the results

#4015 - $15.00 US
Received 11 March 2004; revised 24 May 2004; accepted 25 May 2004

are presented in Fig. 9. Extensive amount of noise in the data near θ = 0°, due to the inherent problems associated with dividing $I'_{obj,p}$ by $I_{obj,p}$ as both values approach zero, resulted in the statistical discarding of these points. Figure 9 shows that a maximum $\eta_0(\theta)$ of 76.4 % was measured for θ = -10°.

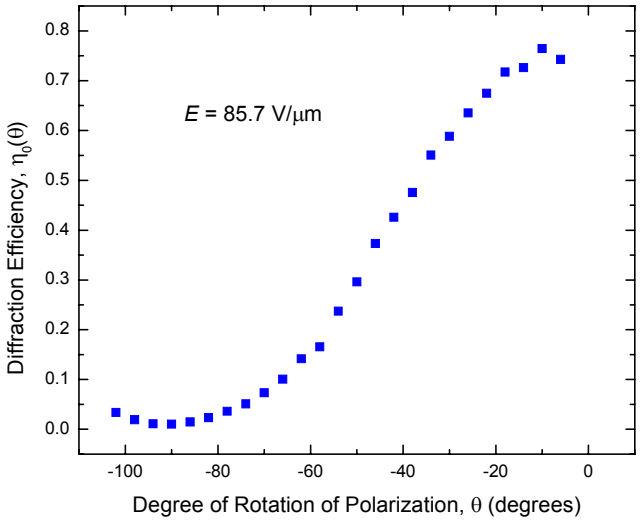

Fig. 9. The external steady state diffraction efficiency, η_0, determined via the novel forward FWM geometry as a function of the rotation of the polarization of I_{obj}, θ. E = 85.7 V/μm.

A characteristic feature of the PR effect is that the refractive index grating created in the medium is spatially shifted with respect to the light intensity pattern of the writing beams resulting in asymmetric energy transfer between the writing beams [11]. While this phenomenon is not relevant to the application of image correction as presented in this study, the observance of TBC is considered conclusive proof of the PR mechanism [11] and the TBC data is included to serve to provide a comprehensive characterization of this material under the given experimental conditions. The strength of the energy transfer depends upon the coupling gain coefficient

$$\Gamma = L^{-1}\left[\ln(\gamma_0\kappa) - \ln(\kappa + 1 - \gamma_0)\right], \tag{6}$$

where L is the effective sample thickness, κ is the ratio of the writing beam intensities before the sample, and γ_0 is the beam-coupling ratio, defined as $\gamma_0 = P_1/P_0$ where P_1 is the intensity of the signal with the pump, and P_0 is the intensity of the signal without the pump [29].

For TBC characterizations the same experimental configuration was employed as that used in the imaging and FWM experiments with the following exceptions: The half-wave plate $(\lambda/2)_1$ is configured such that the output radiation is either *p*-polarized or *s*-polarized and $(\lambda/2)_2$ is appropriately adjusted such that the output polarization remains identical to the input polarization. In addition, the polarizing beam-splitter was removed in order to monitor the intensity of transmitted beams at PD1 and PD2. A typical trace obtained in the TBC experiment is presented in Fig. 10(a) and the results for the TBC experiments are presented in Fig. 10(b). For E = 85.7 V/μm, it was determined that Γ = 75 cm^{-1}. From a practical point of view, the optical gain Γ must exceed the optical loss α (absorption, scattering, reflection, etc.) of the PR sample. Here the optical loss was determined, in the absence of I_{obj} and any externally applied voltage, according to the equation

#4015 - $15.00 US
Received 11 March 2004; revised 24 May 2004; accepted 25 May 2004

$$\alpha = L^{-1}\left[\log\left(I_{\text{ref}} / I'_{\text{ref}}\right)\right] , \qquad (7)$$

where I_{ref} is the intensity of the reference beam before the sample and I'_{ref} is the intensity of the reference beam after the sample. In our case the optical loss was ascertained to be $\alpha = 17$ cm^{-1}. Thus, net gain was observed under the present experimental conditions for *p*-polarization. It is noted, however, that the primary objective of this communication is the demonstration of the ability of a PR polymeric composite to clean a badly distorted laser beam and the subsequent retrieval of information carried by such a beam, therefore significant gain of the object beam was not crucial.

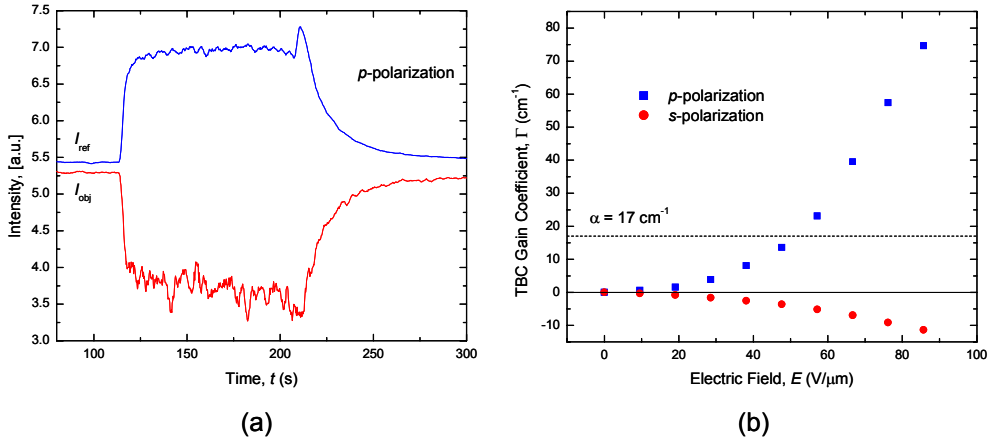

Fig. 10. a) Example of asymmetric energy exchange between laser beams in the TBC experiment. The external electric field $E = 85.7$ V/μm was applied at time $t = 114$ s and turned off at $t = 209$ s, and b) TBC gain coefficient, Γ, as a function of the externally applied electric field, E, for *s*-polarization and *p*-polarization.

4. Conclusions

In conclusion, we have demonstrated, for the first time, the dynamic correction of aberrated images in real-time using a polymeric composite with a fast response time. The current experimental design is extremely capable of restoring a phase aberrated image carrying laser beam to nearly its original quality. Moreover, the ability to reconstruct images in real time has been demonstrated through the translation of the aberrating medium at a variety of speeds. In addition, this technique allows for the correction of constantly changing images, as demonstrated through the oscillating nature of the resolution target. We have also demonstrated that important parameters such as response time, diffraction efficiency and optical gain all retain reasonable values under the current experimental conditions.

Acknowledgments

This work was supported by the Polymer Chemistry branch of the Air Force Office of Scientific Research.

#4015 - $15.00 US Received 11 March 2004; revised 24 May 2004; accepted 25 May 2004